Chemical Engineering Journal 161 (2010) 332–339

Contents lists available at ScienceDirect

Chemical Engineering Journal

journal homepage: www.elsevier.com/locate/cej

In situ studies of structure–reactivity relations in biodiesel synthesis over nanocrystalline MgO

Janine M. Montero[a], D. Rob Brown[b], Pratibha L. Gai[a], Adam F. Lee[c,*], Karen Wilson[c,**]

[a] Department of Chemistry, University of York, York YO10 5DD, UK
[b] Department of Chemistry, University of Huddersfield, Huddersfield, UK
[c] School of Chemistry, Cardiff University, Cardiff CF10 3AT, UK

ARTICLE INFO

Article history:
Received 7 May 2009
Received in revised form
25 September 2009
Accepted 21 December 2009

Keywords:
Biodiesel
Catalysis
MgO
In situ XPS
TEM

ABSTRACT

High temperature processing of solvothermally synthesised MgO nanoparticles promotes striking changes in their morphology, and surface chemical and electronic structure. As-prepared NanoMgO comprised ~4 nm cubic periclase nanocrystals, interspersed within an amorphous $Mg(OH)(OCH_3)$ matrix. These crystallites appear predominantly (1 0 0) terminated, and the overall material exhibits carbonate and hydroxyl surface functionalities of predominantly weak/moderate base character. Heating promotes gradual crystallisation and growth of the MgO nanoparticles, and concomitant loss of $Mg(OH)(OCH_3)$. In situ DRIFTS confirms the residual precursor and surface carbonate begin to decompose above 300 °C, while in situ XPS shows these morphological changes are accompanied by the disappearance of surface hydroxyl/methoxide species and genesis of O^- centres which enhance both the surface density and basicity of the resulting stepped and defective MgO nanocrystals. The catalytic performance in tributyrin transesterification with methanol is directly proportional to the density of strong surface base sites.

1. Introduction

Biodiesel is a clean, renewable fuel source that is viewed as a viable alternative to dwindling petroleum-based diesel resources, and may play an important role in reducing CO_2 emissions over the next 50 years [1]. It is currently synthesised via the transesterification of natural animal fats or plant oils with C_1–C_2 alcohols [2]. Commercial biodiesel production currently employs soluble base catalysts, such as Na or K alkoxides, to transesterify the C_{14}–C_{20} triglyceride (TAG) components of plant oils into their fatty acid methyl esters (FAMEs) which constitute biodiesel, forming glycerol as a by-product [3]. Subsequent aqueous quench cycles, required to isolate the biodiesel product, are problematic due to soap formation and emulsification [4], however complete extraction of the soluble catalyst is essential since it corrodes vehicle fuel tanks and injectors. These processing steps also contaminate the glycerol by-product, rendering it unusable without costly purification. There is therefore much academic and commercial interest in the development of solid base catalysts as alternative green chemical technologies, eliminating quenching steps and associated contaminated water waste, and enabling process intensification via continuous biodiesel production.

A range of solid base catalysts have been investigated for biodiesel synthesis over the past decade, including alkaline earth [5–7] transition metal [8,9] and lanthanide oxides [10], amino acid functionalised polymers [11], and alkali promoted micro- and mesoporous silicates/aluminates [12,13]. However, while a number of important themes have emerged from these studies, such as the impact of trace free fatty acid or water impurities, choice of reaction temperature, and chemical stability towards leaching [14,15], there remains little consensus on how to quantify and tune surface basicity, and thereby direct the design of more active catalysts. Several studies have identified MgO as a promising catalyst for soyabean and vegetable oil transesterification [13,16–18]. MgO is a particularly interesting material, since it is has been the subject of extensive theoretical and experimental surface science studies [19–21], exhibits exciting optical properties [22] and architectures [23,24], and can be synthesised in a variety of presentation formats (including nanosheets [25,26] and nanoparticles [27–29]). We recently showed that nanocrystalline MgO is a promising tuneable, solid base catalyst for triglyceride transesterification with methanol [30]. In this study, we utilise a variety of in situ spectroscopic and microscopic methodologies to track the thermal evolution of strong base sites in MgO nanoparticles, in order to better understand how catalyst processing influences the resulting transesterification activity in the conversion of glyceryl tributyrate (tributyrin) to methyl butanoate (Scheme 1).

* Corresponding author at: School of Chemistry, Cardiff University, Main Building, Cardiff CF10 3AT, UK. Tel.: +44 2920874778; fax: +44 2920874778.
** Co-corresponding.
E-mail address: leeaf@cardiff.ac.uk (A.F. Lee).

1385-8947/$ – see front matter © 2010 Elsevier B.V. All rights reserved.
doi:10.1016/j.cej.2009.12.035

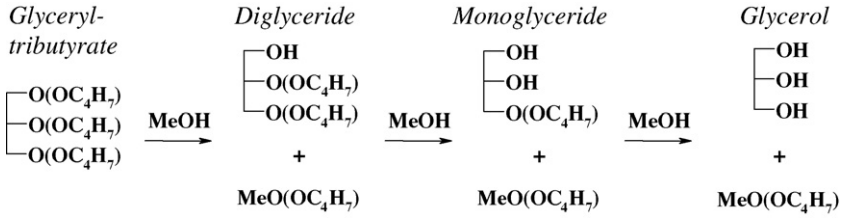

Scheme 1. Transesterification of tributyrin with methanol to methyl butanoate and glycerol.

2. Materials and methods

2.1. Catalyst synthesis

Nanoparticulate MgO catalysts were prepared from the methoxide precursor adapting the method described by Utamapanya et al. [27]. A 10 wt% solution of magnesium methoxide in methanol was prepared by first dissolving Mg ribbon (Aldrich, ≥99.5%) in methanol under N_2. The resulting methoxide solution was hydrolyzed overnight in the presence of toluene and the resulting sol transferred to a stainless steel Büchi Limbo autoclave which was pressurized to 100 psi N_2 at room temperature. This mixture was slowly heated at 1 °C min^{-1} to 265 °C to produce a supercritical methanol atmosphere, which was maintained for 10 min, after which the autoclave was vented. The resulting white powder precursor, $Mg(OH)(OCH_3)$, was dried in an oven at 120 °C for 2 h and then stored in a desiccator prior to either in vacuo annealing or ex situ calcination at 300 °C to create the parent material NanoMgO, which was then calcined at temperatures between 400 and 700 °C (indicated by NanoMgO-XXX).

2.2. Base titration

Pulse chemisorption experiments were carried out on a Quantachrome ChemBET 3000 instrument. In a typical pulse chemisorption experiment, samples were prepared in situ by heating NanoMgO to the required temperature for 5 h under a 90 ml/min flow of He. Base site titration was performed by pulsing 50 μl doses of carbon dioxide (99%, BOC) onto the oxide surfaces at 40 °C until all available base sites were saturated. The CO_2 level in the gas stream was monitored after passing through the sample, and compared to a calibration value corresponding to a full 50 μl pulse. When these signals matched then no more CO_2 could be chemisorbed by the sample.

2.3. Adsorption calorimetry

Flow adsorption calorimetric studies were made in a flow-through differential scanning calorimeter (Setaram DSC111) connected to gas flow and switching systems. The gas flow rates were controlled by automated mass flow controllers. Samples (~20–40 mg) were held on a glass frit in a vertical silica glass sample tube in the calorimeter and activation of the samples was effected at 150 °C under a 5 ml/min flow of He. In a typical experiment, samples at 40 °C are exposed to a sequence of pulses of probe gas (1% CO_2 in He), delivered to the carrier gas stream from a 1 ml sample loop using a two position Valco valve with an automated micro-electric actuator. The heat output associated with interaction between CO_2 and sample is detected with the DSC and the concentration of CO_2 in the gas flow downstream of the DSC is measured with a Hiden mass spectrometer gas analyser (HPR 20). A pulse delay of 30 min is employed for the baselines to stabilise. The net amount of CO_2 irreversibly adsorbed from each pulse can then be determined by comparing the MS signal during each pulse with a signal recorded during a control experiment through a blank sample tube at the same temperature.

2.4. In situ DRIFTS

DRIFTS analysis was performed using a Thermo Electron corporation Nicolet Avatar 370 MCT with Smart Collector accessory. Measurements were performed in a water-cooled, temperature-controlled Thermo Scientific environmental chamber fitted with a ZnSe window and connected to electronic mass flow controllers. Spectra were recorded in vacuo (10^{-2} Torr) as a function of temperature, with samples equilibrated for 5 min prior to spectral acquisition.

2.5. In situ XPS

Surface analysis was performed on a Kratos HSi spectrometer using a monochromatic Al Kα X-ray source (1486.6 eV), with an analyser pass energy of 40 eV operated at normal emission. Sample charging was minimised using a magnetic charge neutralisation system, and binding energies were referenced to adventitious carbon. Temperature-dependent O and C 1s XP spectra and O KLL Auger spectra were recorded within the main analysis chamber while maintaining a base pressure of 1×10^{-9} Torr. Analysis and fitting were performed using CasaXPS 2.3.5, adopting a common mixed Gaussian-Lorentzian lineshape (70:30) for all spectra. FWHM and peak positions were fixed across the anneal series, and the minimum number of peaks required to achieve a good fit was used in all cases.

2.6. In situ aberration corrected TEM

Calcination studies were carried out at the 1 Å (0.1 nm) level in a double aberration corrected (AC)- JEOL 2200FS FEG TEM/STEM, modified with a wide gap (~4.3 mm)-objective pole piece, and pumping system equipped with gas tolerant turbo molecular pumps and a Gatan hot stage.

2.7. Catalytic testing

Transesterification was performed in a stirred Radley's batch reactor at 60 °C. Reaction tubes were charged with 0.01 mol (3 ml) of glyceryl tributyrate (Sigma–Aldrich, 98%), 0.0025 mol (0.587 ml) of dihexyl ether (Sigma–Aldrich, 97%) as an internal standard and 0.3036 mol (12.5 ml) of methanol. Samples were used as prepared, without further activation. Reactions were typically run with 50 mg of catalyst for 6 h with 0.2 ml aliquots of the reaction mixture periodically withdrawn over this period. Sampling was also performed after 24 h to establish the maximum possible conversion under these reaction conditions. Analysis was performed on a Varian CP-3800 gas chromatograph, fitted with a flame ionisation detector (FID), a CP-8400 AutoSampler and VF-1 capillary column (film thickness 0.25 μm, i.d. 0.32 mm, length 30 m).

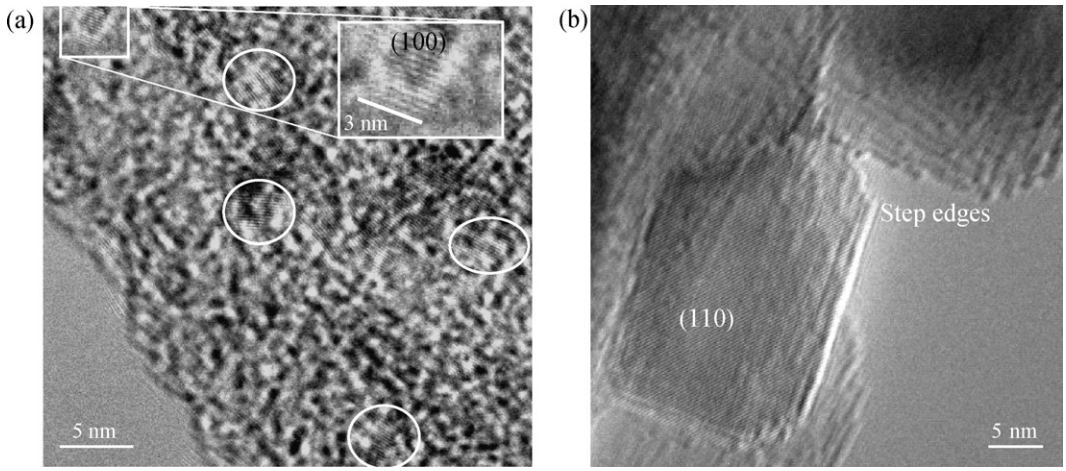

Fig. 1. (a) TEM micrograph of as-prepared NanoMgO showing (1 0 0) terminated crystallites. (b) TEM micrograph of 700 °C in vacuo annealed NanoMgO showing stepped, cuboidal crystallites.

3. Results and discussion

The bulk and surface characteristics of fresh and thermally processed NanoMgO were followed in vacuo by between room temperatures and 700 °C. As previously reported [30], in situ XRD shows the as-prepared material comprised a mix of periclase MgO and residual Mg(OH)(OCH_3) precursor, the latter decomposing above 300 °C to yield a crystalline periclase powder. This transformation is accompanied by thermal sintering: in situ TEM (Fig. 1a), reveal the fresh NanoMgO contains well-defined cubic MgO nanocrystallites of around 3–5 nm width, embedded within an amorphous matrix presumably consisting of the Mg(OH)(OCH_3) precursor observed by powder XRD. High-resolution micrographs identified the crystal termination as exposing predominantly (1 0 0) surfaces. In vacuo annealing above 300 °C induced several morphological transformations. The amount of amorphous material progressively disappears, accompanied by growth of large cuboidal nanoparticles, suggesting migration from the former to latter. Simultaneously, the preferred surface termination switches in favour of (1 1 1) or (1 1 0) atom arrangements. This restructuring promotes the formation of low coordination defect sites, clearly visible as facetted steps at the corners of these larger nanocrystals, and also the genesis of dislocations propagating along the <111> directions within the surface exposed crystallographic faces. The limiting particle size was ~18 nm following a 700 °C anneal (Fig. 1b). Comparative physicochemical data for our NanoMgO series and a range of related MgO nanocrystals are summarised in Table 1.

The surface functionality was subsequently probed by DRIFTS. Fig. 2 shows the evolving surface IR spectra of the NanoMgO sample as a function of in vacuo annealing temperature. The freshly prepared material exhibits strong bands arising from the Mg(OH)(OCH_3) precursor (υ_{O-Mg-O} = 867 cm^{-1}; υ_{C-O} = 1100 cm^{-1}; υ_{OH} = 3250 and 3750 cm^{-1}; υ_{CH3} = 2800–3000 cm^{-1}), physisorbed water, and also surface carbonate which likely arises from CO_2 sequestration from air during sample transfer. The precursor and carbonate bands weaken significantly above 200 °C, falling close to the detection limit following processing ≥400 °C. Since these phases are undetectable by XRD, they must be associated with either amorphous or surface confined regions. Note some C=O features persists up to 700 °C, evidenced by the weak 1100 cm^{-1} band which has been previously assigned to the symmetric stretch of monodentate bound carbonate [31]. This may reflect a contribution from residual carbonate monolayers formed via readsorption of evolved CO_2 during DRIFTS measurements which were performed under a comparatively poor dynamic vacuum (1×10^{-2} Torr). Bulk $MgCO_3$ is know to persist up to 600 °C [32], while even low background CO_2 pressures are known to stabilise $CaCO_3$ thermal decomposition at temperatures above 700 °C [33].

Further insight into the surface composition and electronic properties was derived from XPS, which is particularly sensitive to the outermost layers of any solid. Overall surface compositions are shown in Table 2, and were essentially temperature independent, indicating no net desorption of decomposed surface species, only their redistribution in different forms. The persistence of surface carbon at higher temperatures is indicative of stable carbonate/carbonaceous residues. The resulting fitted C 1s spectra of NanoMgO are shown in Fig. 3a, following sequential in vacuo annealing and analysis without air-exposure. Two principal components are present under all conditions, a high binding energy state centred at 288.8 eV characteristic of $MgCO_3$, and a low binding energy state at 283.8 eV due to adventitious carbon. Fresh NanoMgO also contains a third state at 284.9 eV, which may be assigned to an etheric carbon (–O-C-R) arising from residual methoxide. This methoxide component rapidly decomposes above 400 °C, much of this transforming to carbonaceous fragments. Fig. 3b shows that surface carbonate persists up to 700 °C, as indicated by the IR of NanoMgO-700, the stronger XP signals reflecting the far higher surface sensitivity of XPS which cannot easily discriminate bulk CO_3 from monolayer CO_3. We propose the strong CO_3^{2-} IR band in Fig. 2 arises from carbonate multilayers formed on the fresh sample, which are thermally unstable with respect

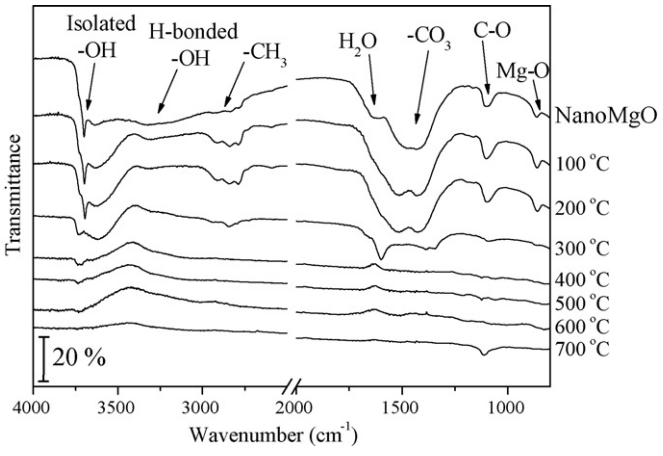

Fig. 2. DRIFTS spectra of NanoMgO as a function of in vacuo annealing temperature.

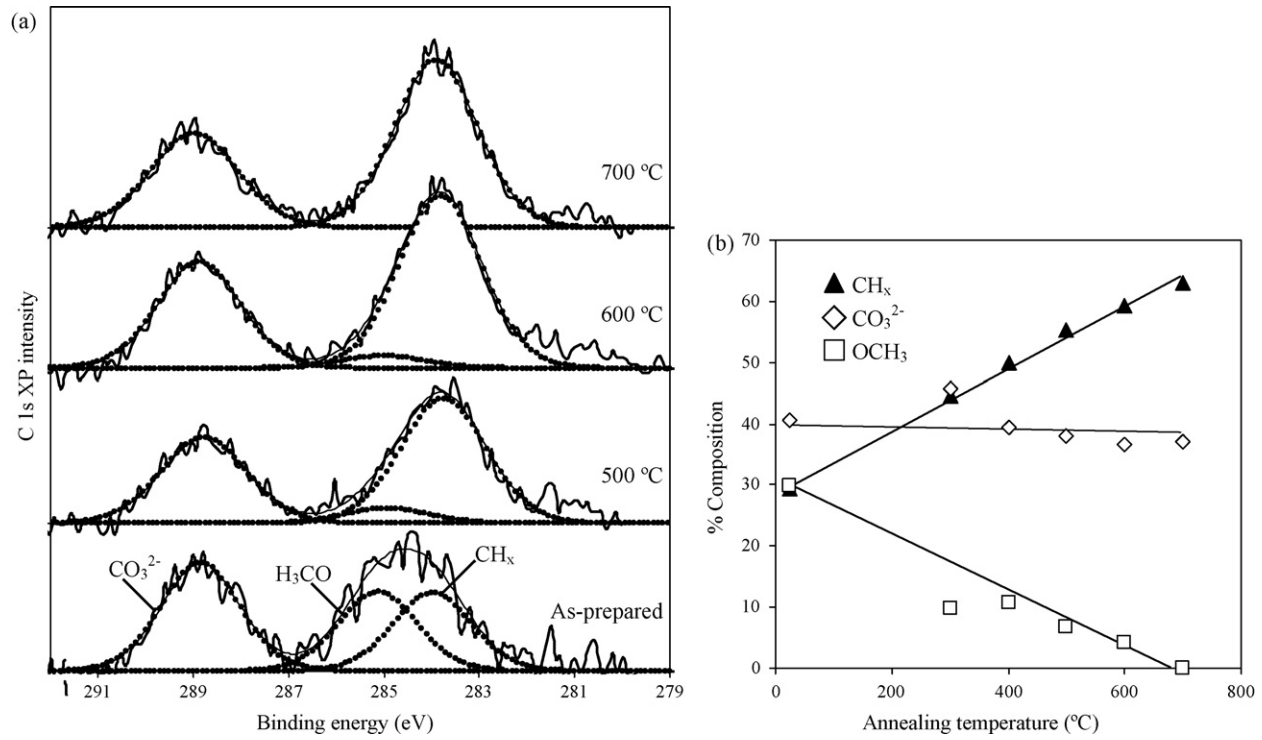

Fig. 3. (a) C 1s XP spectra of NanoMgO as a function of in vacuo annealing temperature. (b) Fitted C 1s spectral components of NanoMgO as a function of in vacuo annealing temperature.

to a truncated/monolayer carbonate phase barely detectable by vibrational spectroscopy. Corresponding O 1s spectra are shown in Fig. 4a which reveal two partially resolved features centred at 528.4 and 530.5 eV. The low binding energy state may be readily assigned to O^{2-}, while the chemical shift of the second state is consistent with surface carbonate [34], but may also contain contributions from surface hydroxyl/methoxide species for which the reference literature is poor reflecting the complexity of synthesising and characterising pure standards. This hypothesis was confirmed by calculating the 530.5 eV peak area attributable to

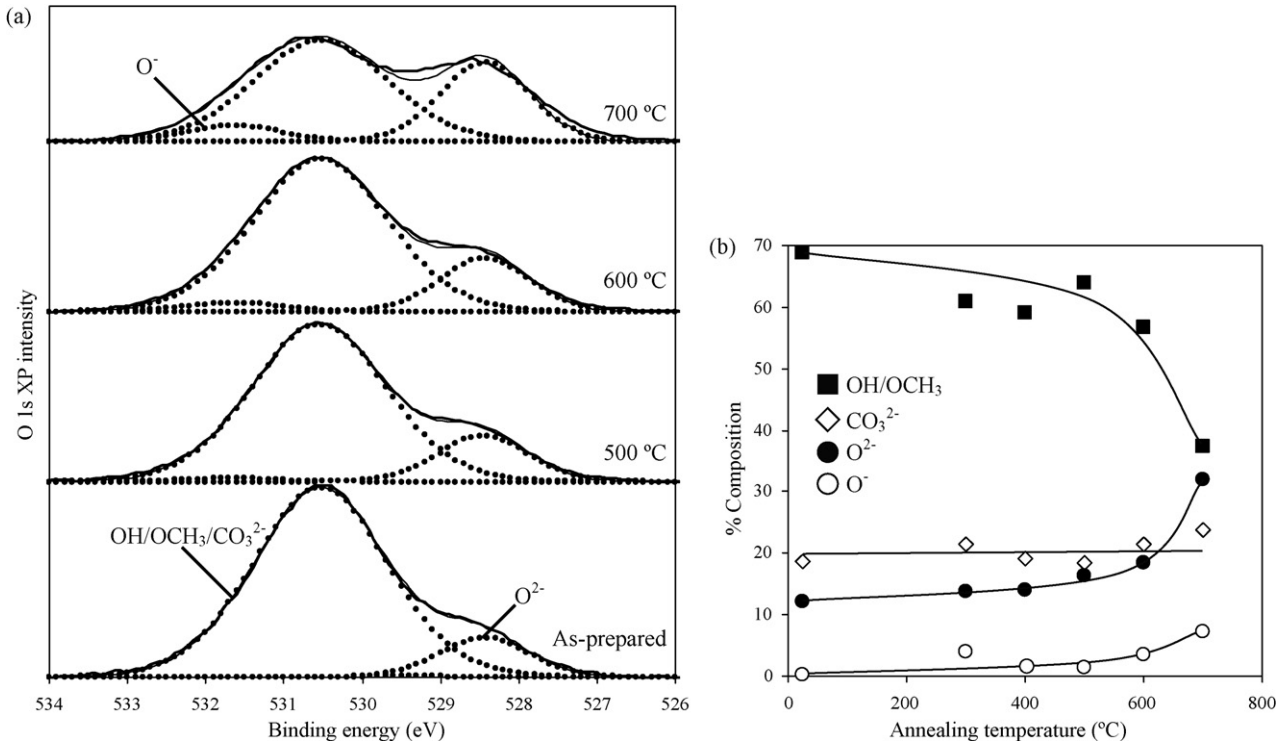

Fig. 4. (a) O 1s XP spectra of NanoMgO as a function of in vacuo annealing temperature. (b) Fitted O 1s spectral components of NanoMgO as a function of in vacuo annealing temperature.

Table 1
Physicochemical properties of MgO nanoparticles.

Sample	Surface area /$m^2\,g^{-1}$	Crystallite size/nm	Bulk phases	Exposed facets	Crystallite morphology	C=O IR bands/cm^{-1}	Oxide O 1s binding energy/eV	Auger parameter/eV	Reference
NanoMgO	580	2.9	Periclase, $Mg(OH)(OCH_3)$	(100)	Cubic	1504, 1404, 1100	527.9	1038.91	This work
NanoMgO-400	360	5.0	Periclase	–	–	1507, 1414	528.0	1039.13	This work
NanoMgO-500	250	7.4	Periclase	(100), (110), (111)	Eroded cube	1509, 1415, 1100	528.2	1039.33	This work
NanoMgO-600	140	10.6	Periclase	–	–	1509, 1414	528.1	1039.39	This work
NanoMgO-700	80	16.0	Periclase	(100), (110), (111)	Eroded cube	1509, 1416, 1100	528.3	1039.50	This work
Commercial MgO	30	50–100	Periclase	–	Cubic	1505, 1422	528.7	1039.20	This work
Commercial $Mg(OH)_2$	160	–	Brucite	–	Sheets	1505, 1414	–	–	This work
Comm. $MgCO_3$	70	–	Magnesite	–	Flakes	1512, 1481, 1421	–	–	This work
$Mg(OH)(OCH_3)$	1090	–	$Mg(OH)(OCH_3)$	–	Sheets	1460 (br)	–	–	This work
AP-MgO	300–500	3.6–7.3	Periclase	Primarily (110)	Polyhedral	1590, 1510, 1415, 865	–	–	[16,23,27,28]
CP-MgO	130–250	100[a]	Periclase	Primarily (100)	Hexagonal plates	1385, 1335, 850	–	–	[16,23,28]
MgO nanosheets	200	50–200[a]; 3–5[b]	Periclase	(111)	Sheets/plates	1706, 1654, 1523, 1449, 1396, 1332, 1239	–	–	[2,25,26]
MgO nanocubes	–	3–10	Periclase	(100)	Cubic	–	–	–	[22]
MgO nanowires	140	3×10^4[a]; 10[b]	Periclase	(100)	Wires	–	–	–	[24]

[a] Diameter.
[b] Thickness.

Table 2
Surface compositions of in vacuo annealed NanoMgO.

Sample	Atomic %		
	O	C	Mg
NanoMgO	63.7	10.3	26.0
NanoMgO-400	61.6	9.9	28.5
NanoMgO-500	67.3	11.4	21.4
NanoMgO-600	63.7	13.2	23.0
NanoMgO-700	62.0	13.6	24.4

CO_3^{2-} from the corresponding C 1s CO_3^{2-} (288.8 eV) carbonate signal, including appropriate sensitivity factors; at all temperatures carbonate is only a minor contributor to this 530.5 eV state. Fig. 4b confirms the persistence of residual surface carbonate up to 700 °C, and the loss of surface hydroxyl/methoxide species and simultaneous exposure of the underlying surface oxide. Detailed analysis of the O 1s spectra also uncovered the emergence of a weak, very high binding energy state following high temperature anneals at 531.6 eV. A good spectral fit could only be achieved by the inclusion of this additional component, which we assign to electron deficient O^- ions. The high temperature required to form a significant quantity of this surface species (700 °C) is also in excellent agreement with predicted O^- formation temperatures from early XPS and HREELS studies [34,35]. Such O^- species are often also associated with anion vacancy generation (F centres), with both moieties implicated as catalytically active sites in C–H activation, e.g. oxidative methane coupling [34,36,37] and correlate well with the appearance of atomic defects seen by TEM.

In order to assess the impact of crystallite growth and surface vacancy generation upon the basic properties of MgO, chemical titration and adsorption flow calorimetery were conducted using CO_2 as an acidic probe molecule. The saturation CO_2 adsorption capacity (i.e. maximum surface base site density) of NanoMgO was probed as a function of pre-annealing temperature. Fig. 5 shows a sharp rise in the total available surface base sites (normalised to BET surface area) on heating from 300 to 500 °C, which we associate with defect formation, followed by a much slower increase up to 700 °C coincident with O^- formation. The site density for NanoMgO of $4 \times 10^{+17}\,m^{-2}$ is similar to previous observations for MgO [38]. Insight into the base strength distribution of NanoMgO was obtained from temperature-programmed CO_2 desorption profiles, and exemplar spectra are shown in Fig. 6. These surface area normalised TPD spectra reveal two well-defined CO_2 desorption peaks for NanoMgO at 100 and 300 °C, which have been asso-

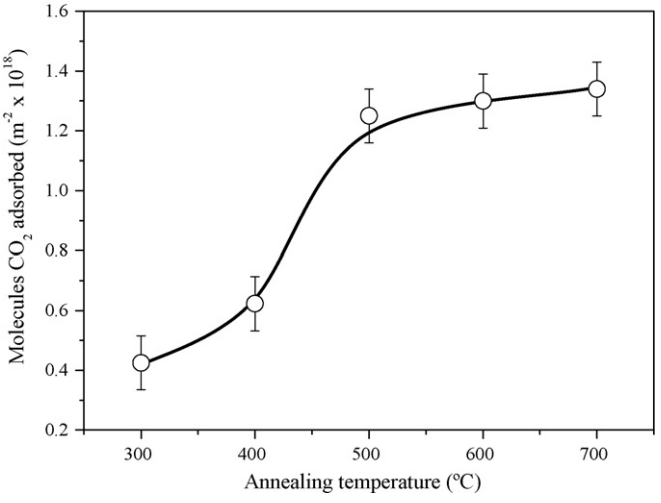

Fig. 5. Saturation CO_2 coverage of pre-annealed NanoMgO nanocrystals at 313 K.

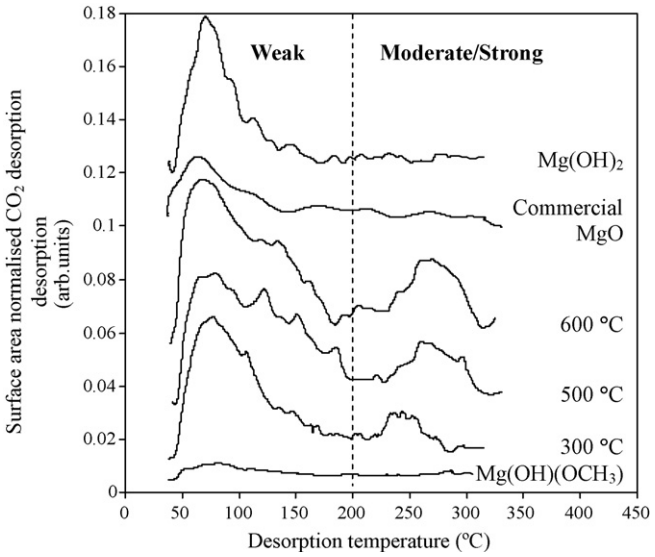

Fig. 6. Surface area normalised CO_2 desorption from pre-annealed NanoMgO nanocrystals saturated with CO_2 at 313 K.

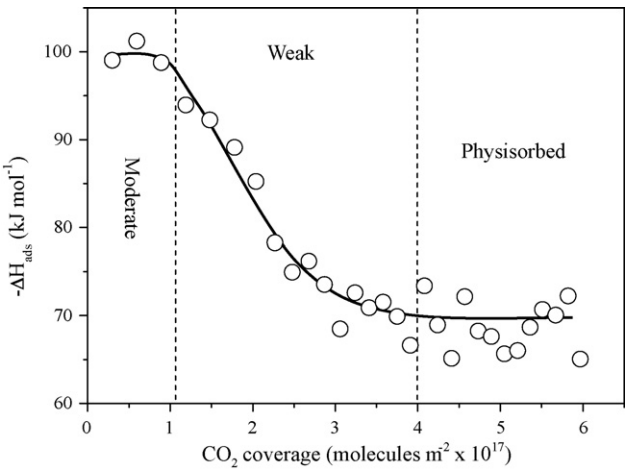

Fig. 8. Differential heat of adsorption of CO_2 as a function of coverage on NanoMgO.

ciated with weakly basic surface hydroxyls and moderate base strength stoichiometric $Mg^{2+}O^{2-}$ surface species [16]. The unprocessed precursor exhibits little CO_2 chemisorption, indicating the presence of few (weak) base sites. Even moderate calcination at 300 °C dramatically increases the CO_2 desorption yield, giving rise to a large number of weak base sites and a significant fraction of stronger O^-/O^{2-} species, the latter favoured by higher temperature pretreatments. In contrast, commercial MgO and $Mg(OH)_2$ are both only weakly basic, with the former possessing few base sites in accordance with its low surface area (Table 1). The integrated peak intensities in Fig. 7 confirm a steady rise in the overall density of surface base sites with annealing temperature, mirrored by a monotonic increase in the proportion of strong base sites from ~10–20%. Solid basic strengths for the NanoMgO were further quantified via calorimetry (Fig. 8) which reveal an initial CO_2 adsorption enthalpy around $-102\,kJ\,mol^{-1}$. This value is in good agreement with literature values for polycrystalline MgO [38,39] and Mg–Al hydrotalcites [40] which range between -107 and $-120\,kJ\,mol^{-1}$, while the saturation CO_2 coverage of $\sim 4 \times 10^{17}\,m^{-2}$ is very close to that derived from our independent pulse titration data. Two adsorption regimes can be identified. Approximately one fifth of titratable sites have moderate basicity, with $\Delta H_{ads}(CO_2)$ lying between -95 and $102\,kJ\,mol^{-1}$. We attribute these to surface O^{2-} species that give rise to the high temperature state in Fig. 6. The remaining CO_2 molecules adsorbed with a monotonically falling heat of adsorption, indicating the fresh NanoMgO exposes a broad distribution of moderate-weak base sites, likely corresponding to geminal and isolated surface hydroxyls.

The catalytic performance of these thermally processed MgO nanoparticles was explored in the transesterification of tributyrin, a useful probe reaction for assessing solid basicity in biodiesel synthesis [6,41]. Resulting reaction profiles are shown in Fig. 9, which in all cases reveal a linear initial portion during the first 2 h, followed by a slower deactivation stage resulting in limiting tributyrin conversions between 60 and 80% after 24 h. At first glance these data suggest that transesterification activity passes through a maximum following pre-annealing at 400 °C, however this neglects the significant drop in surface area accompanying nanoparticle sintering. As we have previously shown, the surface area normalised turnover frequencies (derived from the linear portion of the rate profiles) actually increase sharply with pre-annealing temperature but reach a plateau above 500 °C, beyond which a rise in the density

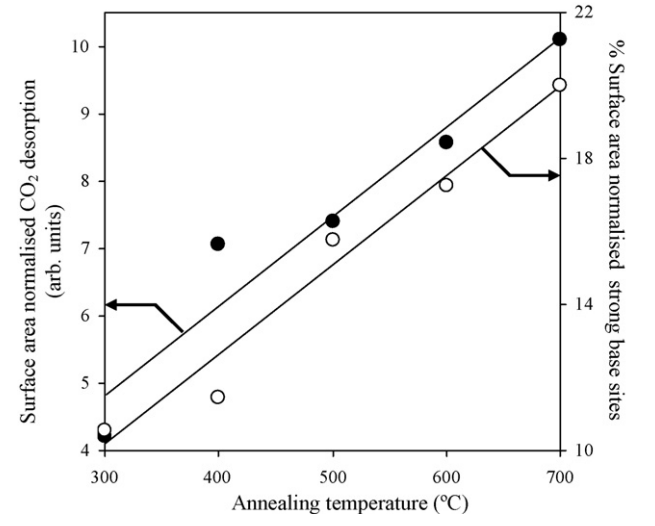

Fig. 7. Total CO_2 yield and proportion of strongly bound CO_2 desorbing from pre-annealed NanoMgO nanocrystals saturated with CO_2 at 313 K.

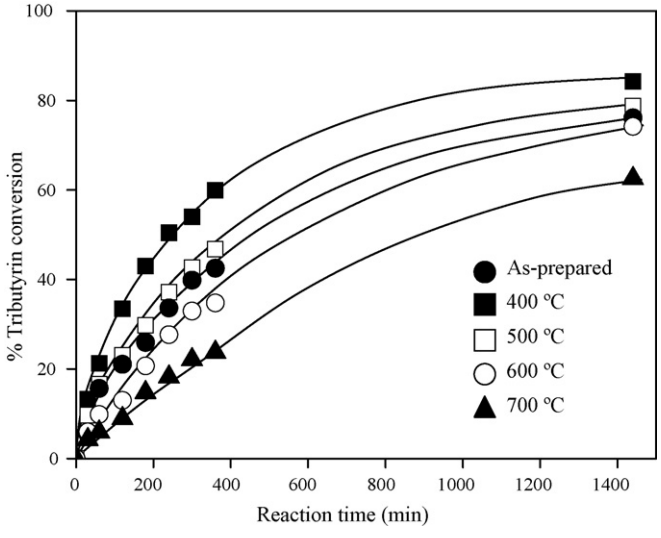

Fig. 9. Tributyrin conversion over a NanoMgO as a function of pre-annealing temperature.

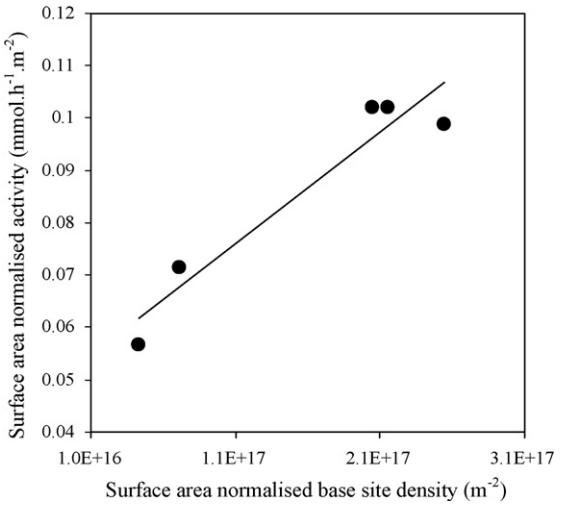

Fig. 10. Dependence of catalytic activity towards tributyrin transesterification on surface density of moderate/strong base sites over freshly prepared and thermally processed NanoMgO.

and base strength of surface sites compensates for the falling surface area [30]. More insight into the impact of thermally induced base site creation upon catalytic activity can be obtained by examining the activity dependence on the number of moderate/strong surface base sites. As anticipated for this relatively facile transesterification, Fig. 10 reveals a direct and strong correlation between the density of stronger base sites (e.g. O^-, O^{2-} or cationic vacancies) at the surfaces of stepped MgO nanoparticles and their resulting reaction rates. The absolute turnover frequency of $\sim$220 h^{-1} (per strong base site) for the most active 700 °C annealed MgO compares favourably with the best recently reported for the transesterification of tributyrin with methanol over activated hydrotalcites [42].

4. Conclusion

The powerful combination of in situ electron microscopy, diffraction and surface spectroscopies enables the thermal evolution of bulk and surface properties of nanocrystalline MgO to be investigated in detail, and the associated solid base character to be optimised for tributyrin transesterification.

Acknowledgements

This work was supported by the Engineering and Physical Sciences Research Council [EP/E013090/1, EP/F063423]. JMM thanks BP Biofuels and EPSRC for the award of a studentship.

AFL thanks the EPSRC for the award of a Leadership Fellowship [EP/G007594/1].

References

[1] A. Demirbas, Progress and recent trends in biodiesel fuels, Energy Convers. Manage. 50 (2009) 14–34.
[2] F. Ma, M.A. Hanna, Biodiesel production: a review, Bioresour. Technol. 70 (1999) 1–15.
[3] G. Vicente, M. Martinez, J. Aracil, Integrated biodiesel production: a comparison of different homogeneous catalysts systems, Bioresour. Technol. 92 (2004) 297–305.
[4] K. Narasimaharao, A.F. Lee, K. Wilson, Catalysis in production of biodiesel: a review, Chem. Rev. 1 (2007) 1–12.
[5] M. Kouzu, T. Kasuno, M. Tajika, S. Yamanaka, J. Hidaka, Active phase of calcium oxide used as solid base catalyst for transesterification of soybean oil with refluxing methanol, Appl. Catal. A 334 (2008) 357–365.
[6] R.S. Watkins, A.F. Lee, K. Wilson, Li-CaO catalysed tri-glyceride transesterification for biodiesel applications, Green Chem. 6 (2004) 335–340.
[7] C. Reddy, V. Reddy, R. Oshel, J.G. Verkade, Room-temperature conversion of soybean oil and poultry fat to biodiesel catalyzed by nanocrystalline calcium oxides, Energy Fuels 20 (2006) 1310–1314.
[8] D.E. López, J.G. Goodwin Jr., D.A. Bruce, S. Furuta, Esterification and transesterification using modified-zirconia catalysts, Appl. Catal. A 339 (2008) 76–83.
[9] Z. Yang, W. Xie, Soybean oil transesterification over zinc oxide modified with alkali earth metals, Fuel Process. Technol. 88 (2007) 631–638.
[10] X. Li, G. Li, Y. Guo, Y. Guo, Y. Wang, Z. Zhang, X. Liu, Y. Wang, A novel solid superbase of Eu_2O_3/Al_2O_3 and its catalytic performance for the transesterification of soybean oil to biodiesel, Catal. Commun. 8 (2007) 1969–1972.
[11] U. Schuchardt, R.M. Vargas, G. Gelbard, Alkylguanidines as catalysts for the transesterification of rapeseed oil, J. Mol. Catal. A: Chem. 99 (1995) 65–70.
[12] M. Verziu, M. Florea, S. Simon, V. Simon, P. Filip, V.I. Parvulescu, C. Hardacre, Transesterification of vegetable oils on basic large mesoporous alumina supported alkaline fluorides—evidences of the nature of the active site and catalytic performances, J. Catal. 263 (2009) 56–66.
[13] A. Corma, S. Iborra, S. Miquel, J. Primo, Catalysis for the production of fine chemicals, J. Catal. 173 (1998) 315–321.
[14] B. Freedman, E.H. Pryde, T.L. Mounts, Variables affecting the yields of fatty esters from transesterified vegetable oils, J. Am. Oil Chem. Soc. 61 (1984) 1638–1643.
[15] C.S. MacLeod, A.P. Harvey, A.F. Lee, K. Wilson, Evaluation of the activity and stability of alkali-doped metal oxide catalysts for application to an intensified method of biodiesel production, Chem. Eng. J. 135 (2007) 63–70.
[16] M. Verziu, B. Cojocaru, J. Hu, R. Richards, C. Ciuculescu, P. Filip, V.I. Parvulescu, Sunflower and rapeseed oil transesterification to biodiesel over different nanocrystalline MgO catalysts, Green Chem. 10 (2008) 373–381.
[17] G. Arzamendi, E. Arguiñarena, I. Campo, S. Zabala, L.M. Gandía, Transesterification of soybean oil with methanol catalyzed by basic solids, Catal. Today 133–135 (2008) 548–554.
[18] M. Di Serio, M. Cozzolino, M. Giordano, R. Tesser, P. Patrono, E. Santacesaria, From homogeneous to heterogeneous catalysts in biodiesel production, Ind. Eng. Chem. Res. 46 (2007) 6379–6384.
[19] S. Coluccia, A.J. Tench, R.L. Segall, Surface structure and surface states in magnesium oxide powders, J. Chem. Soc. Faraday Trans. I 74 (1978) 1769–1779.
[20] G. Pacchioni, J.M. Ricart, F. Illas, Ab initio cluster model calculations on the chemisorption of CO_2 and SO_2 probe molecules on MgO and CaO (1 0 0) surfaces. A theoretical model of oxide basicity, J. Am. Chem. Soc. 116 (1994) 10152–10158.
[21] M. Chiesa, M.C. Paganini, E. Giamello, C. Di Valentin, G. Pacchioni, First evidence of a single-ion electron trap at the surface of an ionic oxide, Angew. Chem. Int. Ed. 42 (2003) 1759–1761.
[22] S. Stankic, M. Müller, O. Diwlad, M. Sterrer, E. Knözinger, J. Barnardi, Size-dependent optical properties of MgO nanocubes, Angew. Chem. Int. Ed. 44 (2005) 4917–4920.
[23] R. Richards, W. Li, S. Decker, C. Davidson, O. Koper, V. Zaikovski, A. Volodin, T. Rieker, K.J. Klabunde, Consolidation of metal oxide nanocrystals. Reactive pellets with controllable pore structure that represents a new family of porous inorganic materials, J. Am. Chem. Soc. 122 (2000) 4921–4925.
[24] A. Subramania, G. Vijaya Kumar, A.R. Sathiya Priya, T. Vasudevan, Polyol-mediated thermolysis process for the synthesis of MgO nanoparticles and nanowires, Nanotechnology 18 (2007) 225601–225605.
[25] K. Zhu, J. Hu, C. Kübel, R. Richards, Efficient preparation and catalytic activity of MgO(1 1 1) nanosheets, Angew. Chem. Int. Ed. 45 (2006) 7277–7281.
[26] J. Hu, K. Zhu, L. Chen, C. Kübel, R. Richards, MgO(1 1 1) nanosheets with unusual surface activity, J. Phys. Chem. C 111 (2007) 12038–12044.
[27] S. Utamapanya, K.J. Klabunde, J.R. Schlup, Nanoscale metal oxide particles/clusters as chemical reagents. Synthesis and properties of ultrahigh surface area magnesium hydroxide and magnesium oxide, Chem. Mater. 3 (1991) 175–181.
[28] K.J. Klabunde, J. Stark, O. Koper, C. Mohs, D.G. Park, S. Decker, Y. Jiang, I. Lagadic, D. Zhang, Nanocrystals as stoichiometric reagents with unique surface chemistry, J. Phys. Chem. 100 (1996) 12142–12153.
[29] K.J. Klabunde (Ed.), Nanoscale Materials in Chemistry, Wiley-Interscience, New York, 2001.
[30] J.M. Montero, P. Gai, K. Wilson, A.F. Lee, Structure-sensitive biodiesel synthesis over MgO nanocrystals, Green Chem. 11 (2009) 265–268.
[31] J.V. Stark, D.C. Park, I. Lagadic, K.J. Klabunde, Nanoscale metal oxide particles/clusters as chemical reagents. Unique surface chemistry on magnesium oxide as shown by enhanced adsorption of acid gases (sulfur dioxide and carbon dioxide) and pressure dependence, Chem. Mater. 8 (1996) 1904–1912.
[32] N. Khan, D. Dollimore, K. Alexander, F.W. Wilburn, The origin of the exothermic peak in the thermal decomposition of basic magnesium carbonate, Thermochim. Acta 367–368 (2001) 321–333.
[33] M. Maciejewski, J. Bałdyga, The influence of the pressure of the gaseous product on the reversible thermal decomposition of solids, Thermochim. Acta 92 (1985) 105–108.
[34] T. Karasuda, K.-I. Aika, Characterization of electron deficient oxide ion of heat treated MgO for activation of methane, Bull. Chem. Soc. Jpn. 71 (1998) 1999–2003.
[35] M.C. Wu, C.M. Truong, K. Coulter, D.W. Goodman, Investigations of active sites for methane activation in the oxidative coupling reaction over pure and Li-promoted MgO catalysts, J. Catal. 140 (1993) 344–352.
[36] T. Ito, J.H. Lunsford, Synthesis of ethylene and ethane by partial oxidation of methane over lithium-doped magnesium oxide, Nature 314 (1985) 721–722.

[37] T. Ito, J. Wang, C.H. Lin, J.H. Lunsford, Oxidative dimerization of methane over a lithium-promoted magnesium oxide catalyst, J. Am. Chem. Soc. 107 (1985) 5062–5068.
[38] A. Auroux, A. Gervasini, Microcalorimetric study of the acidity and basicity of metal oxide surfaces, J. Phys. Chem. 94 (1990) 6371–6379.
[39] G.A.H. Mekhemer, S.A. Halawy, M.A. Mohamed, M.I. Zaki, Qualitative and quantitative assessments of acid and base sites exposed on polycrystalline MgO surfaces: thermogravimetric, calorimetric and in-situ FTIR spectroscopic study, J. Phys. Chem. B 108 (2004) 13379–13386.
[40] F. Winter, X. Xia, B.P. Hereijgers, J.H. Bitter, A. Jos van Dillen, M. Muhler, K.P. de Jong, On the nature and accessibility of the Brønsted-base sites in activated hydrotalcite catalysts, J. Phys. Chem. B 110 (2006) 9211–9218.
[41] D.G. Cantrell, L.J. Gillie, A.F. Lee, K. Wilson, Structure–reactivity correlations in MgAl hydrotalcite catalysts for biodiesel synthesis, Appl. Catal. A 287 (2005) 183–190.
[42] Y. Xi, R.J. Davis, Influence of water on the activity and stability of activated Mg–Al hydrotalcites for the transesterification of tributyrin with methanol, J. Catal. 254 (2008) 190–197.